Materials Research Proceedings 41 (2024) 2065-2074 https://doi.org/10.21741/9781644903131-228

Experimental analysis of burr formation during Ti6Al4V drilling

DEBARD Benoit[1,a], REY Pierre-André[1,b], CHERIF Mehdi[1,c*], CHIRON Thierry[1,d], SOMMIER Alain[1,e], CHAVATTE Theo[1,f]

[1]I2M, Bordeaux University, 33405 Talence, France

[a]benoit.debard@ensam.eu, [b]pierre-andre.rey@ensam.eu, [c]mehdi.cherif@ensam.eu
[d]thierry.chiron@u-bordeaux.fr, [e]alain.sommier@u-bordeaux.fr, [f]theo.chavatte@u-bordeaux.fr

Keywords: Ti6Al4V, Drilling, Burr, Temperature, Wear

Abstract. To improve the assembly process of aeronautical structures by the mean of One-Way Assembly strategies (no deburring of metallic parts before the installation of final fasteners), it is mandatory to monitor the burr size of drilled holes. Indeed, burrs can have a significant effect on the fatigue life of structures. It was shown that cracks are initiated from exit burrs. This paper presents an experimental analysis of the burr geometry through cutting forces and thermal imaging measurements. The effect of the tool wear on burr geometry is also analyzed to identify phenomena occurring during burr formation.

Introduction

In order to lighten planes without reducing their mechanical properties, aeronautic industry developed hybrid structures (metal 1 with metal 2 or metal with carbon) composed of low-density material, such as Aluminum, Titanium and Carbon Fiber Reinforced Polymer (CFRP). The mechanical assembly of these structures requires to drill a lot of holes which are made through the entire stack. In metallic parts, the drilling process produces burrs at part interfaces. These burrs can reduce the fatigue life of aeronautic structures depending on their size [1,2]. As shown by Eynian et al. [3], cracks are initiated from exit burrs. So, industrials have to manage them to preserve the mechanical properties of hybrid structures.

To do this, industrials must disassemble structures, clean and deburr interfaces and then re-assemble them before installing the final fasteners. This strategy includes several non-added value phases: disassembling, deburring and re-assembling. The One-Way Assembly is an assembly strategy in which the final fastener is installed just after the hole is drilled, thus avoiding those non-added value phases. But, to deploy this strategy, it is mandatory to monitor the burr size at stack interfaces, particularly with titanium plates, where the largest burrs occur.

In the literature, most of authors only look at the burr geometry, while few of them studied the whole formation of the burr [2,4–6], whereas it is essential to fully understand burr formation phenomena. Gillespie [4] detailed formation mechanisms of both entrance and exit burrs. These burrs have different formation mechanisms, leading to two different burr morphologies [3]. The Fig. 1 shows the exit burr formation scheme during the drilling process proposed by Gillespie [4] and completed by Kim et Dornfeld [7]. According to these authors, burr formation starts at a critical thickness t_0 where the tool tip starts deforming the material of the exit surface (Fig. 1 (a)). A cap is formed in front of the tool during burr formation, and it is removed when the tool corners reach the exit surface (Fig. 1 (f)). The deformed material remaining on the part is called a “burr”.

Most of the studies on burrs are focusing on the exit burr. To understand the formation of exit burrs, several authors investigated the influence of many parameters, such as cutting conditions, material properties and cutting angles [2,4–13]. Patil et al. [12] show that titanium burr height increases with the cutting speed and the feed rate. Kim et al. [2] show that the burr type can be different between two different materials. Dornfeld et al. [6] show that the tip angle influences titanium burr size. Rimpault et al. [13] show that the axial force F_z and the torque M_z have both a

significant effect on titanium burr height. Only few authors studied the influence of temperature on burr geometry [14], but not on burr formation.

This paper presents the experimental analysis of exit burr geometry during the drilling of the titanium alloy Ti6Al4V. Cutting forces, temperature, burr height and burr width have been measured at different level of tool wear. The objective is to understand and explain the evolution of the burr geometry with tool wear by measuring the cutting forces and the temperature.

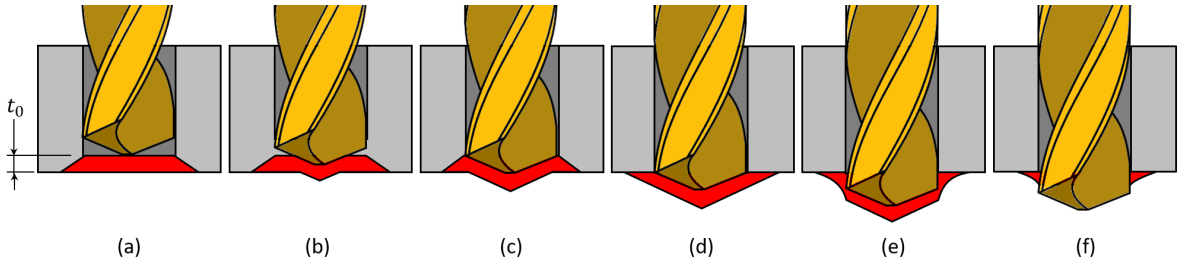

Fig. 1: Drilling burr formation [4,7]

Experimental procedure

Materials. Tests were carried out on a CNC machine, using a two-lip twisted tool with a diameter of 6.35 mm, shown with Fig. 2. It is a TiAlN-coated tool, with a tip angle of 140 degrees. Holes are drilled in samples made of Ti6Al4V titanium alloy, with a thickness of 6.1 mm. All the tests were performed with the same tool.

During the tests, cutting forces were measured using the Kistler tool holder rotating dynamometer 9171A, and exit surface temperature was measured using the thermal camera FLIR A6750 SLS. Burr height and burr width were measured after the tests using the optical 3D microscope Brüker Alicona Infinite Focus G5plus.

Protocol. The experimental setup is shown with Fig. 3. In blue is the CNC spindle, where the Kistler tool holder is mounted in. Forces are measured with a frequency of 2000 Hz.

In green is the optical system that includes the infrared camera. The camera has an integration time of 0.3 s and it was calibrated with a black corpse from 50 °C to 600 °C. The camera is aligned with the tool through a golden mirror inclined at 45 degrees, which has a reflectance of 0.98. The optical path is composed of black tubes to limit as much as possible any noise during thermal measurements. At the end of the optical path, a Potassium Bromide window is placed to avoid any pollution due to chips and lubrication. The window has a transmittance of 0.9.

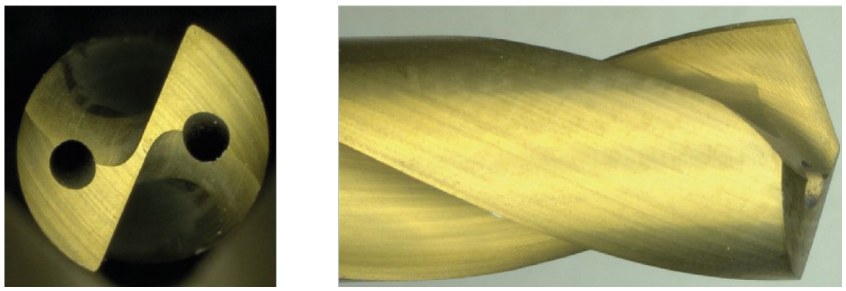

Fig. 2: Tool used during the tests

To realize an accurate measurement with a thermal camera, it is necessary to be perpendicular to what is measured. Otherwise, the emissivity will decrease and the temperature will be underestimated. But it is still possible to compare measurements with the same angle regarding the camera. So, the analysis of thermal measurements during the burr formation is still possible.

In orange is the sample support, that allows the infrared camera to target the sample exit surface. The support was designed to hold two samples: one with the exit surface painted in black (paint

RAL9005), and the other without paint. The black paint allows a better measurement of the temperature. Indeed, it has a reflectance inferior to 0.1, so an emissivity superior to 0.9 [15]. But, as the black paint has a non-neglectable thickness, it perturbate burr size measurements. To avoid these uncertainties, burr measurements were done only on the virgin sample, and thermal measurements only on the painted sample. Both samples have a thickness of 6.1 mm.

Tests are composed of two main phases: the "Measure" phase and the "Wear" phase. The tool wear is considered neglectable during the "Measure" phase, while the purpose of the "Wear" phase is to wear the tool. During the "Measure" phase, tests are performed at 25 m/min cutting speed and a feed rate of 0.06 mm/rev with MQL lubrication. Eight holes are performed, four on the painted sample and four on the virgin sample. Forces and temperature are measured during this phase. During the "Wear" phase, tests are performed with the same feed rate and lubrication, but at a cutting speed of 40 m/min. The sample used is 20 mm thick and 18 holes are drilled on it. Only forces are recorded during this phase.

The "Measure" phase was performed for four wear levels of the tool. The first level corresponds to a new tool. The wear level increases by 1 for each "Wear" phase performed (wear level 2 = 1 "Wear" phase performed, etc…). The last "Measure" phase was performed after 3 "Wear" phase. As the thickness of the sample is not the same during the "Wear" phase and the "Measure" phase, the wear is represented by the cutting length in the results section. The protocol is resumed with the Fig. 4.

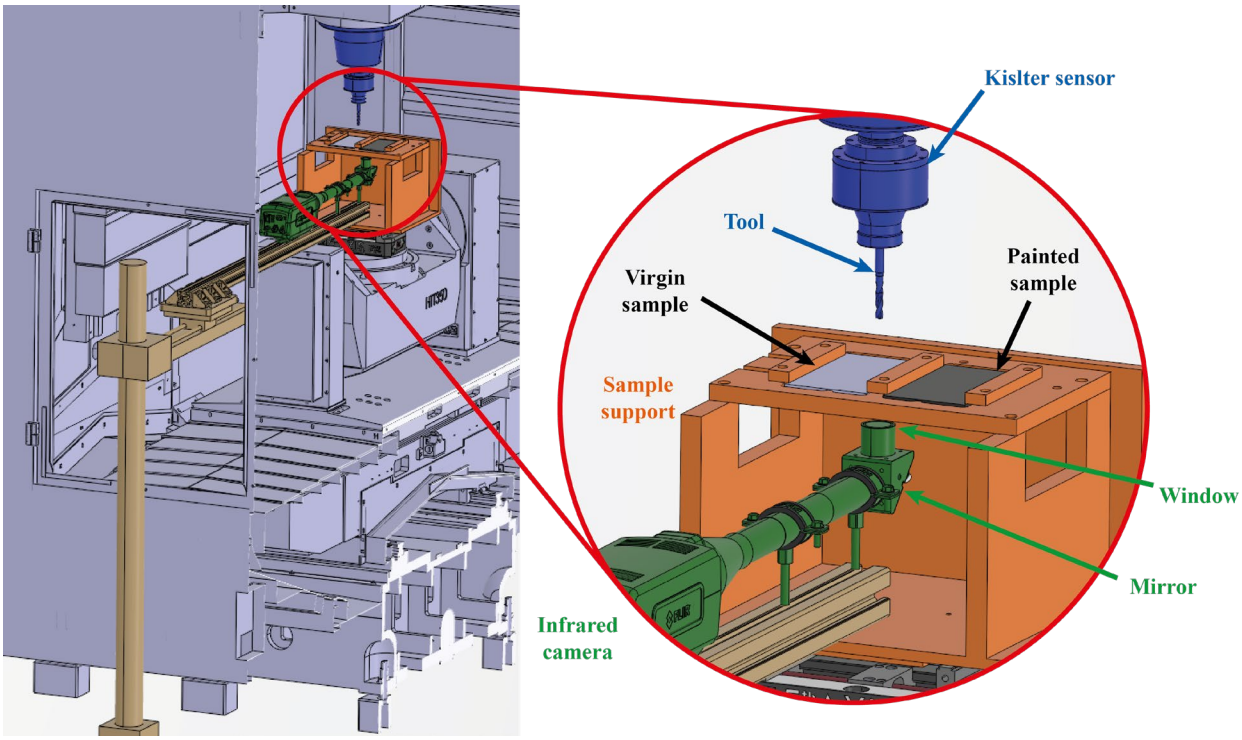

Fig. 3: Experimental setup

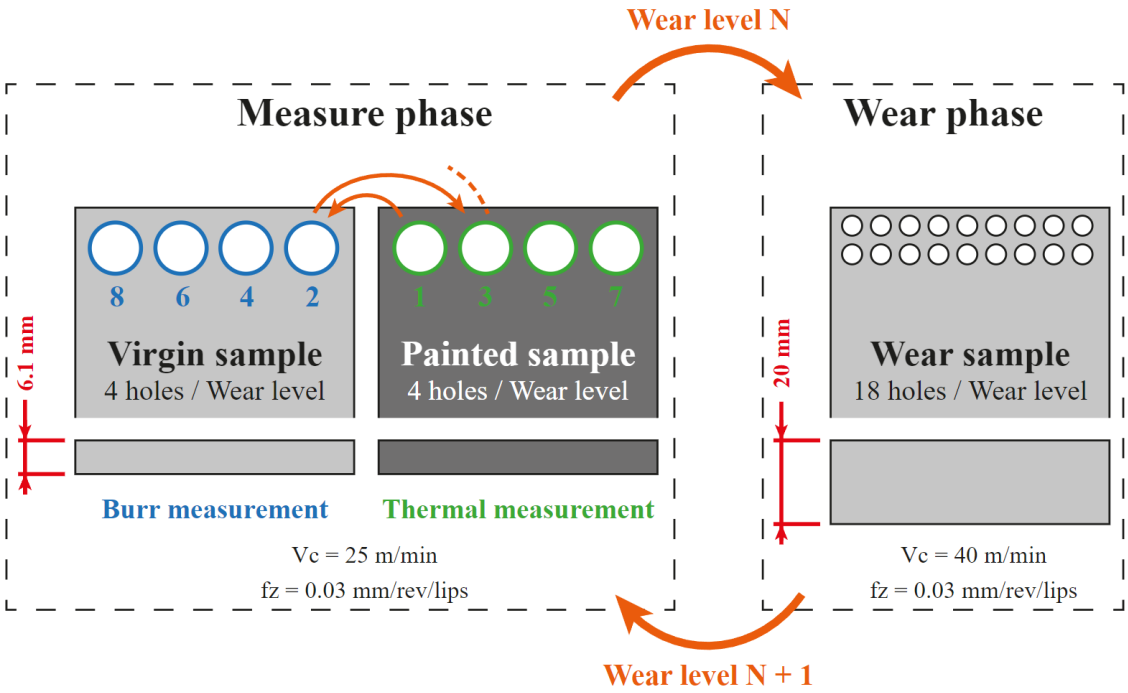

Fig. 4: Tests protocol

Results and Discussion

In this section, results of tool wear, cutting forces, exit surface temperature and burr geometry measurements are first presented separately. Then, a correlation between all these results is established.

Tool wear. The Fig. 5 shows the tool at each wear level. It shows that the main wear mode is adhesive wear. Indeed, it is possible to notice a lot of material adhesion at tool corners, forming a built-up-edge (marked in red in Fig. 5). This built-up-edge modifies significantly the tool macro-geometry at corners and margins. Indeed, the tip length increases from 1.05 mm (wear level 1) to 1.2 mm (wear level 4). Moreover, the tool wear is not symmetrical, leading to cutting tool imbalance.

This figure shows that the tool tip and the middle of the cutting edges have no significant wear. Indeed, at point M (marked in green in Fig. 5), the edge acuity increases slightly from 6 µm to 8 µm. Moreover, no wear can be observed on the flank or rake face, whatever the wear level. Some material is stuck on the tool tip, but not enough to modify significantly the tool macro-geometry.

Cutting forces. The curves of the axial force F_z and the torque M_z for all wear levels are represented on Fig. 6. The X-axis was converted from time to depth of the tool tip. This new scale gives a better understanding of the cutting process with regard to the position of the tool in the material. This figure shows a good repeatability of the drilling at each wear level. At wear level 1, the torque M_z shows a change after few holes, due to the running-in effect.

The entrance phase shows no evolution at the tool tip between wear levels, but the corners contribution to forces increases a lot with tool wear. The built-up-edge at tool corners changes locally the tool macro-geometry. Thus, the edge acuity and the tool-workpiece contact are modified, leading to an increase of cutting forces.

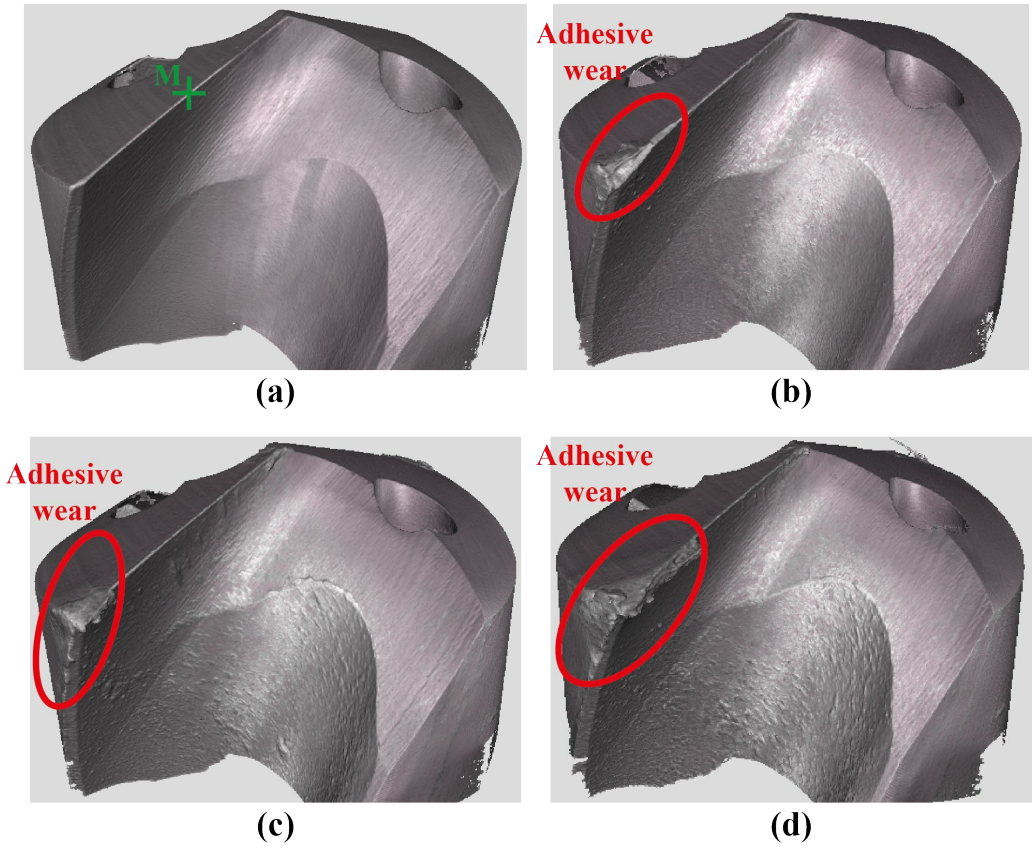

Fig. 5: Top view of the tool at wear level 1 (a), 2 (b), 3 (c) and 4 (d)

This figure also shows that the end of the cutting goes deeper with the tool wear. At wear level 1, the cap breakage occurs at 7.2 mm depth, while at wear level 4, it occurs at 8 mm. The increase of exit length (0.8 mm) is superior to the increase of tip length (0.15 mm), thus the modification of the macro-geometry is not enough to explain this phenomenon. This point is discussed in more detail in the temperature results section.

The Fig. 7 shows the evolution of force amplitude with tool wear. The axial force F_z amplitude was multiplied by 2 between wear levels 1 and 4, while the torque M_z amplitude was multiplied by about 2.5. These curves show no significant evolution between wear levels 2 and 3. The axial force F_z amplitude did not change while the torque M_z amplitude increased slightly. The measured torque M_z depends on several phenomena, such as friction or cutting. The Fig. 5 shows that margins get more wear than corners between wear levels 2 and 3. As margins contribute mainly to the torque M_z, the torque increases more than the axial force F_z.

Temperature. The Fig. 8 (a) shows the evolution with tool wear of the maximal temperature reached during burr formation (square mark), at tool tip (triangle mark) and at tool corners (round mark). This figure shows a good repeatability of measurements for each wear level. The evolution of the temperature is more closed to the torque M_z than the axial force F_z, as the temperature in front of the tool is mainly due to friction.

It also shows that the temperature at tool tip does not increase a lot, while the temperature at tool corners increases a lot, as corners wear faster than the tip. Thus, the maximal temperature is firstly reached near the tool tip (wear level 1), and then near tool corners (wear level 4). The maximal temperature at tip increases by 50°C, while it increases by 300°C at corners. The increase of temperature at tool corners could induce a thermal softening of the material during burr

formation. This softening could explain the increase of exit length observed on cutting force measurements.

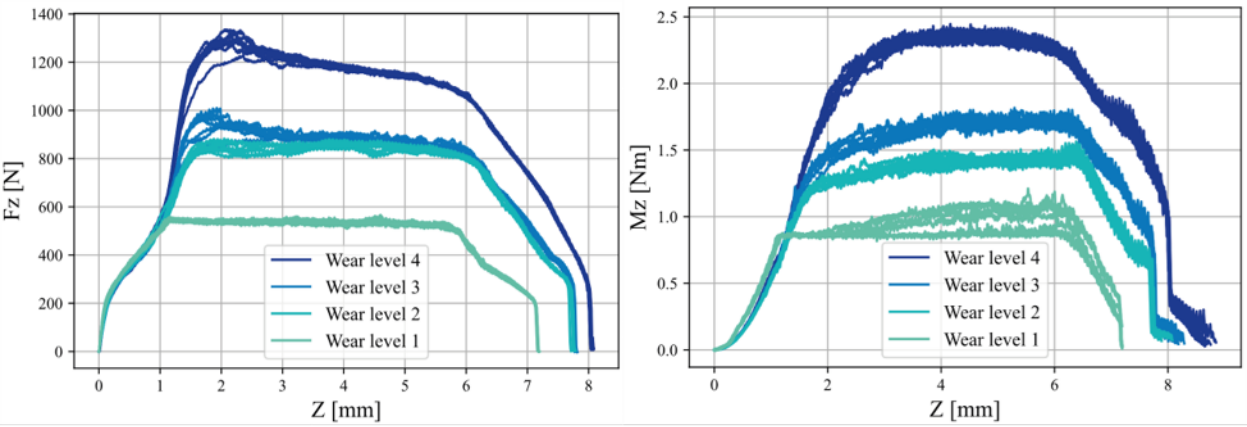

(a) (b)

Fig. 6: Axial force $\boldsymbol{F_z}$ (a) and Torque $\boldsymbol{M_z}$ (b) with tool tip depth $\boldsymbol{Z}$ for all wear levels

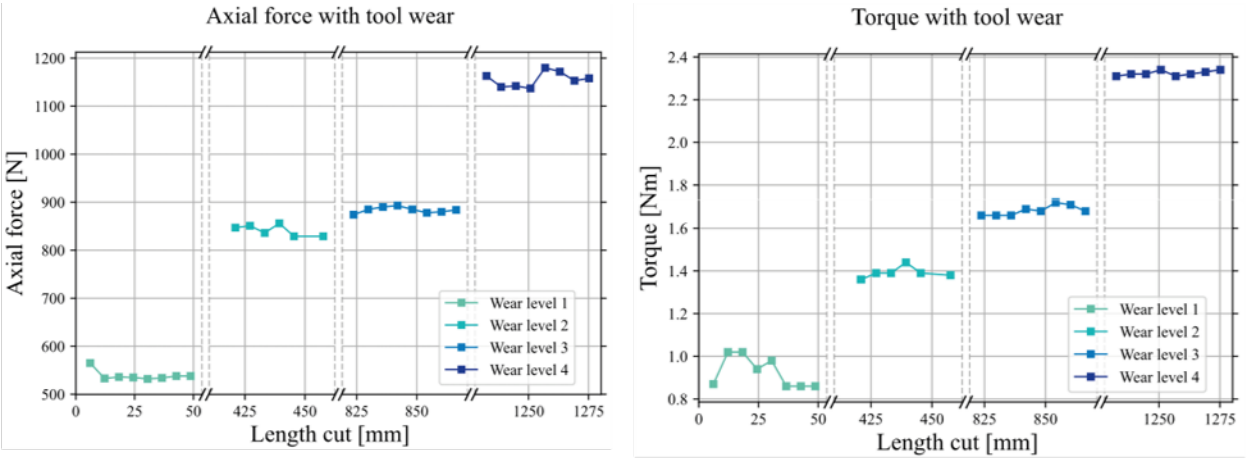

(a) (b)

Fig. 7: Axial force $\boldsymbol{F_z}$ (a) and Torque $\boldsymbol{M_z}$ (b) with tool wear

For each hole, the evolution of the temperature along the hole diameter (see Fig. 8 (b)) has been plotted. Fig. 8 (c) and (d) show respectively the temperature radial profile at 5.5 mm depth, before burr formation, and just before the cap breakage, at the end of burr formation, at wear level 4. Fig. 9 and Fig. 10 are obtained by plotting the temperature radial profile at each depth step on the same graph for respectively wear level 1 and 4. To facilitate the analysis of these figures, the tool tip is marked in magenta and the corners in red. These figures confirm what was told before: when the tool gets wear, the maximal temperature is reached at tool corners.

On these figures, it is possible to notice the particular shape of the profile during the burr formation. The abrupt decrease of temperature corresponds to the cap breakage, which means the end of burr formation. Just before the breakage (see Fig. 8 (d)), the temperature reaches a maximum at tool corners, and a minimum at tool tip. According to Kim et Dornfeld [7], at the end of burr formation, there is no more cutting, only material deformation. Thus, the heat is only generated by the friction between the tool and the material. As the speed is higher at corners than at tool tip, there is more heat generated at corners. That explain the particular shape of the temperature radial profile before the cap breakage.

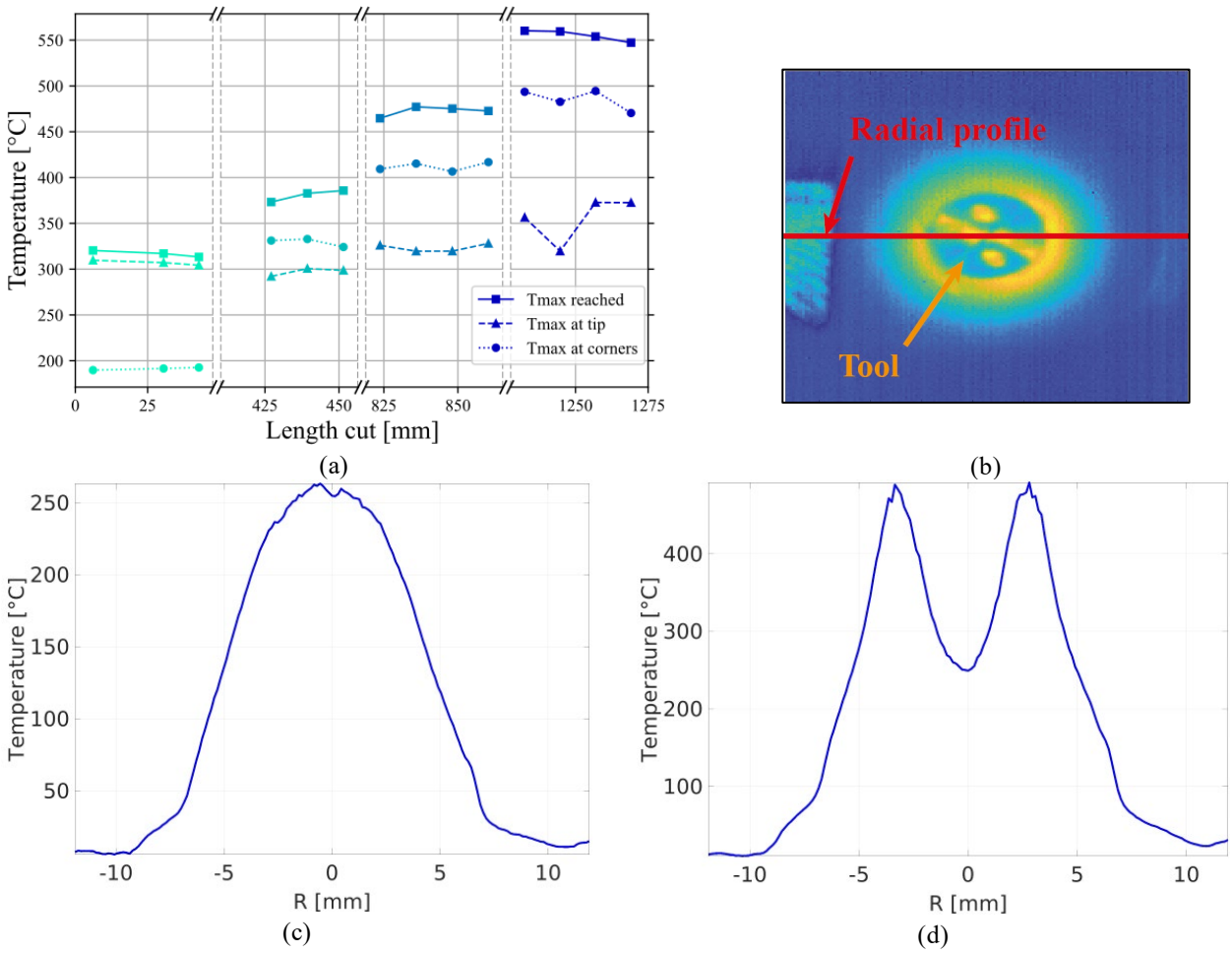

Fig. 8: Maximal temperature reached during burr formation, at tip and at corners with tool wear (a), Radial profile on the exit surface (b), Temperature along the radial profile at 5.5 mm depth (c) and just before the cap breakage (d)

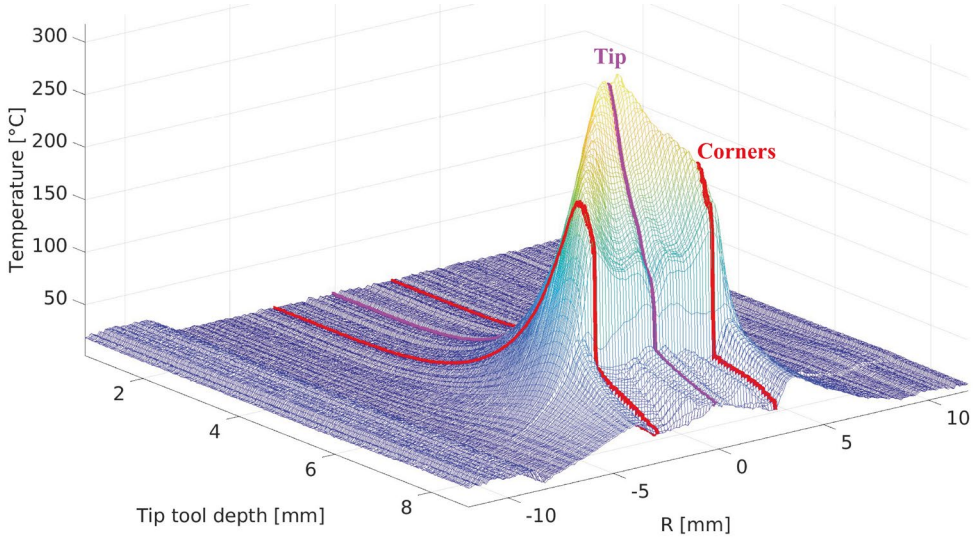

Fig. 9: Temperature along the radial profile with depth at wear level 1

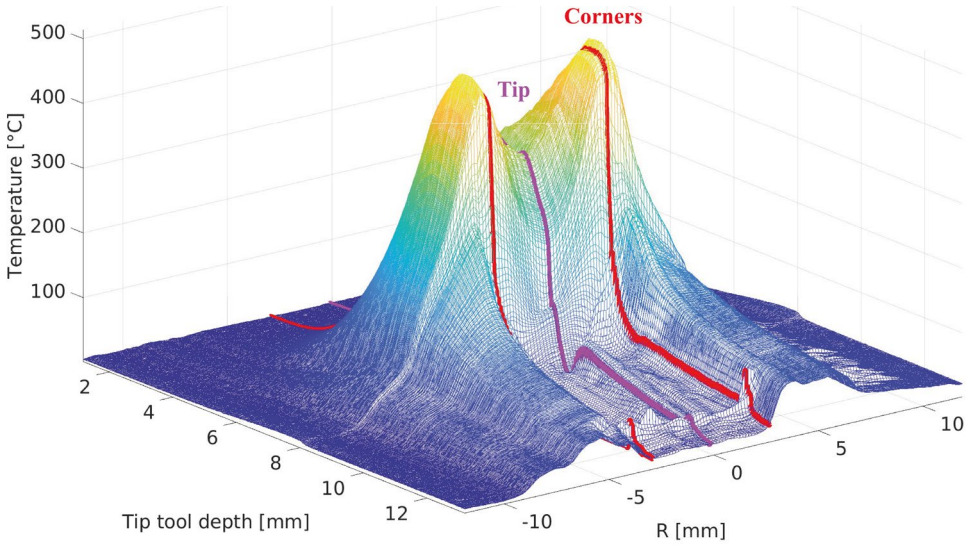

Fig. 10: Temperature along the radial profile with depth at wear level 4

Burr geometry. The Fig. 11 shows the evolution of the burr height and the burr width with tool wear. As burrs are not always regular around the hole, median values are presented on this figure. The error bars correspond to the burr size standard deviation. They are an indicator of the regularity of the burr around the hole.

This figure shows a good repeatability of the results for each wear level. However, the more the burr size goes up, the less it is regular around the hole, especially in terms of width. Because of the non-symmetric wear, the cutting becomes less stable, inducing non regular burrs.

This figure shows that the evolution of the burr height is closer to the evolution of the axial force F_z, while the burr width evolution is closer to the torque M_z. Indeed, the burr height doesn't change between wear level 2 and 3, while the width increases. That shows that the burr height seems less influenced by the torque M_z than the width. As the tool margins are modified due to material adhesion, the way the tool pushes the material perpendicularly to the feed changes too, and so the burr width. The burr height seems not influenced by the margins. That leads to an increase in torque M_z and radial forces. To verify this hypothesis, it is necessary to measure the radial forces.

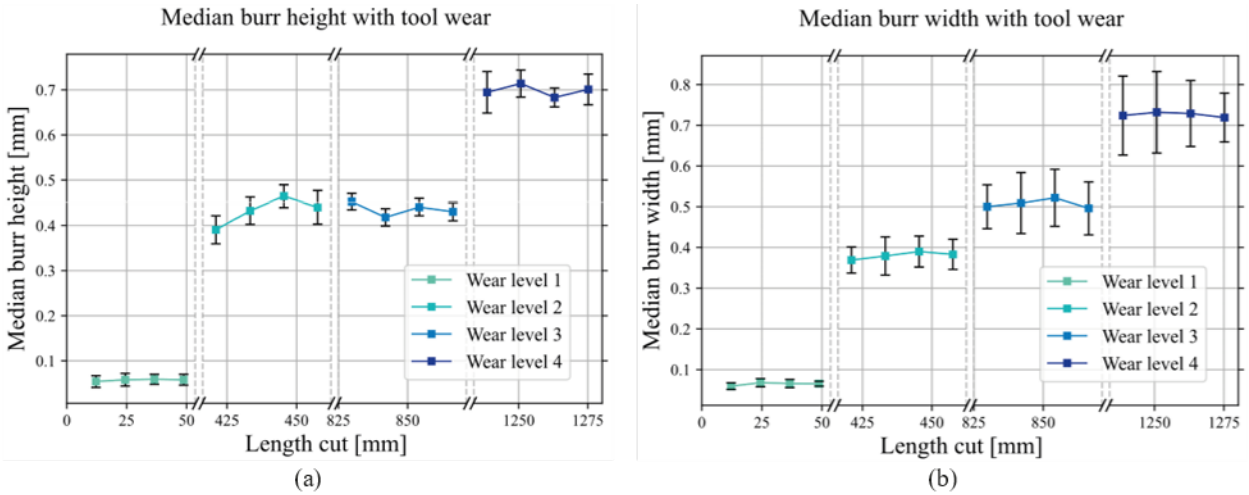

Fig. 11: Median burr height (a) and median burr width (b) with tool wear

Conclusion

The work presented in this paper shows the influence of the tool wear on burrs by measuring cutting forces and temperature. The main wear mode is material adhesion on the cutting edge, mainly at tool corners. This leads to a modification of the tool macro-geometry. The results are synthetized with the Fig. 12.

The thermal measurements show interesting results. At the end of burr formation, the maximal temperature is located at tool corners rather than the tip. Due to the wear, the temperature at corners increases by more than 150 %. At the same time, the burr height increases by 1125 % and the width by 1134 %. In addition to the modification of the tool macro-geometry, a local thermal softening of the material at tool corners can explain the increase of burr size.

The cutting forces measurements show that the burr width seems to be greatly influenced by the torque M_z, and the tool margins. The burr height seems more influenced by the axial force F_z, but not by the margins.

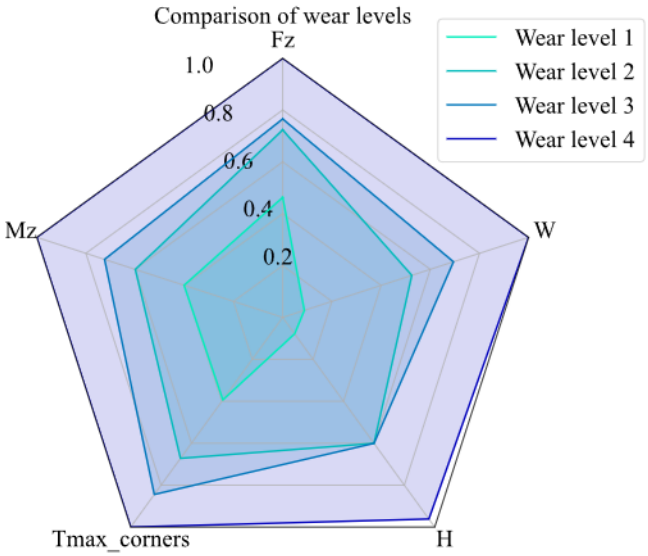

Fig. 12: Synthesis of the results

Acknowledgements

The authors would like to thank the TREFLE department of the laboratory I2M Bordeaux for the supply of the thermal camera, and their help for the preparation of the camera and the treatment of the results.

The authors would also like to thank Airbus Operations SAS for financing the experiments and supplying the tooling and the workpiece material.

References

[1] A.M. Abdelhafeez, S.L. Soo, D.K. Aspinwall, A. Dowson, D. Arnold, The influence of burr formation and feed rate on the fatigue life of drilled titanium and aluminium alloys used in aircraft manufacture, CIRP Annals 67 (2018) 103–108. https://doi.org/10.1016/j.cirp.2018.03.013

[2] J. Kim, S. Min, D.A. Dornfeld, Optimization and control of drilling burr formation of AISI 304L and AISI 4118 based on drilling burr control charts, International Journal of Machine Tools and Manufacture 41 (2001) 923–936. https://doi.org/10.1016/S0890-6955(00)00131-0

[3] M. Eynian, K. Das, A. Wretland, Effect of tool wear on quality in drilling of titanium alloy Ti6Al4V, Part I: Cutting Forces, Burr Formation, Surface Quality and Defects, High Speed Machining 3 (2017) 1–10. https://doi.org/10.1515/hsm-2017-0001

[4] L.K. Gillespie, Burrs produced by drilling, Bendix Corp., Kansas City, Mo. (USA), 1976. https://doi.org/10.2172/7351762

[5] S. Min, D.A. Dornfeld, J. Kim, B. Shyu, FINITE ELEMENT MODELING OF BURR FORMATION IN METAL CUTTING, Machining Science and Technology 5 (2001) 307–322. https://doi.org/10.1081/MST-100108617

[6] D.A. Dornfeld, J.S. Kim, H. Dechow, J. Hewson, L.J. Chen, Drilling Burr Formation in Titanium Alloy, Ti-6AI-4V, (1999).

[7] J. Kim, D. Dornfeld, Development of an Analytical Model for Drilling Burr Formation in Ductile Materials, (2002). https://escholarship.org/uc/item/1cq5k23b (accessed April 4, 2022).

[8] R. Hussein, Vibration Assisted Drilling of Carbon Fiber Reinforced Polymer and Titanium Alloy for Aerospace Application, Thesis, 2019. https://macsphere.mcmaster.ca/handle/11375/24730 (accessed April 4, 2022).

[9] L.K. Lauderbaugh, Analysis of the effects of process parameters on exit burrs in drilling using a combined simulation and experimental approach, Journal of Materials Processing Technology 209 (2009) 1909–1919. https://doi.org/10.1016/j.jmatprotec.2008.04.062

[10] R. Link, Gratbildung und Strategien zur Gratreduzierung bei der Zerspanung mit geometrisch bestimmter Schneide, RWTH Aachen, 1992.

[11] Y.B. Guo, D.A. Dornfeld, Finite Element Modeling of Burr Formation Process in Drilling 304 Stainless Steel, Journal of Manufacturing Science and Engineering 122 (2000) 612–619. https://doi.org/10.1115/1.1285885

[12] R. Patil, S. Shinde, D. Marla, S. Joshi, Experimental analysis of burr formation in drilling of TI-6AL-4V alloy, IJMMS 9 (2016) 237. https://doi.org/10.1504/IJMMS.2016.079591

[13] X. Rimpault, J.-F. Chatelain, J.E. Klemberg-Sapieha, M. Balazinski, Burr height study for drilling carbon epoxy composite / titanium / aluminium stacks, Proceedings of Joint Conference on Mechanical, Design Engineering & Advanced Manufacturing (2014).

[14] I. Rodriguez, P.J. Arrazola, M. Cuesta, F. Pušavec, Hole quality improvement in CFRP/Ti6Al4V stacks using optimised flow rates for LCO2 and MQL sustainable cooling/lubrication, Composite Structures 329 (2024) 117687. https://doi.org/10.1016/j.compstruct.2023.117687

[15] S. Potin, Spectrophotométrie de la matière extra-terrestre, (2020).